

Chirped-pulse multiphoton transitions between Rydberg states

C. W. S. Conover,* M. C. Doogue, and F. J. Struwe

Department of Physics and Astronomy, Colby College, Waterville, Maine 04901

(Received 14 June 2001; published 26 February 2002)

Rydberg atoms in a static electric field provide an experimental system with which many aspects of strong atom-field interactions can be tested. We report measurements of multiphoton transitions in Rydberg states of potassium driven by chirped pulses of rf radiation. Pulses of rf are produced with frequencies swept from 675 to 825 MHz at rates from 0.25 MHz/ns to 7.5 MHz/ns. We present measurements of population transfer in a two-level system as a function of rf field strength and sweep rate. The data is analyzed with a dynamical Floquet model using Landau-Zener transition probabilities; this model accurately describes these transitions.

DOI: 10.1103/PhysRevA.65.033414

PACS number(s): 32.80.Wr, 32.80.Rm, 32.30.Bv, 32.60.+i

I. INTRODUCTION

The efficient excitation of atoms and molecules to particular states is of continuing interest in both physics and chemistry. Use of nearly monochromatic radiation with precisely controlled amplitude and duration can completely drive population to excited states with a π pulse. However, these pulses require precise control over the radiation field and further, atomic motion creates Doppler shifts that limit the effectiveness of π pulses. Over the past decade there has been more interest in the use of frequency and amplitude modulated pulses to efficiently and robustly drive transitions between quantum states. In the technique of stimulated Raman adiabatic passage (STIRAP) [1] two amplitude shaped monochromatic pulses can efficiently and robustly move population within a three-state system with relaxed requirements on the pulse area and frequency, although the frequency difference between the two radiation sources must be precisely controlled. Even more recently there has been interest in extending the STIRAP techniques that have worked for simple three-level systems to more complex ladder systems and to multiphoton transitions [2,3]. Frequency swept (chirped) pulses have been shown theoretically and used experimentally to drive transitions with efficient population transfer in atomic and molecular systems with three or more levels [4–11]. The technique of chirped adiabatic passage (CHIRAP) is insensitive to the pulse area, pulse shape, and exact central frequency of the radiation.

Theoretical work to determine robust laser pulse shapes for ladder climbing by chirped pulses has been carried out using the adiabatic Floquet model and using Landau-Zener analysis of the transition between quasienergy states [12]. To be effective, the theory requires that laser pulses have slowly varying amplitudes and frequencies. However, since the design of frequency and amplitude modulated pulses for use in molecular experiments usually requires ultrafast laser systems, designs for chirped pulses used with realistic models often have frequencies that change on the order of a few cycles, calling into question the use of the adiabatic model.

In this paper, we report on an experimental study of multiphoton transitions driven by frequency swept pulses with constant amplitude in a two-level system. The pulses were

typically 500 cycles long. Specifically, we have measured the population transfer driven by 2, 3, 4, and 5 photon processes as a function of amplitude and chirp of the pulse. We measured the population transfer between states over a wide range of values of the chirp. We have adjusted the frequency sweep from 13% to 26% of the central frequency, and swept the frequencies in times ranging from 450 cycles to ten cycles of the rf.

Using a simple, well-characterized system allows us to carefully compare the experimental results to the direct integration of Schrödinger's equation as well as the adiabatic Floquet model and the associated Landau-Zener probabilities, for transitions driven by chirped pulses. The experimental system that we have used is a pair of Rydberg states [13] in potassium whose energy separation can be tuned by the application of a static electric field. In zero field the $(n+2)s$ state is depressed slightly below the nearly hydrogenic values of the $n\ell$ states ($\ell \geq 3$), where n denotes the principal quantum number and ℓ denotes the orbital angular momentum. In a static field greater than a few V/cm the high- ℓ states are mixed and shifted by a linear Stark effect, and the low- ℓ states are shifted by a quadratic Stark effect. In a large static electric field the energy of the $(n+2)s$ state intersects the manifold of linearly shifted Stark states. The intersection of the $24s$ and lowest state in the $n=22$ manifold is seen in Fig. 1(a).

To label the states, we follow the notation of Bloomfield *et al.* [14] The first state is referred to as an s state because, despite the fact that angular momentum is not a good quantum number in the field, the wave function of this state remains essentially unchanged below the crossing with the Stark manifold. The manifold state that the s state first intersects is labeled by its parabolic quantum number n_1 as the $n,3$ state because it connects to the nf state in zero field. This state is a superposition of all states with $\ell \geq 3$ and thus is not a state of definite parity. The energy levels of these two states, which are referred to as the diabatic states, can be parametrized as

$$W_1 = W_{(n+2)s} = -\frac{1}{2} \alpha^s E^2, \quad (1.1a)$$

$$W_2 = W_{n,3} = W_o - kE, \quad (1.1b)$$

*Electronic address: cwconove@colby.edu

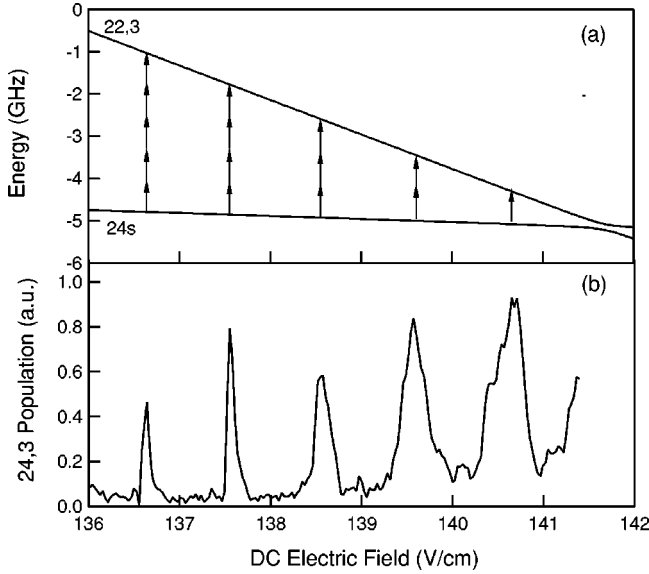


FIG. 1. Figure showing (a) the energies of the $24s$ and $22,3$ states of potassium in a static electric field showing the avoided crossing, $\Omega_o/2\pi=138.5$ MHz, at 141.7 V/cm and (b) the upper-state population after a $1\text{-}\mu\text{s}$ pulse of unchirped 750-MHz radiation with an amplitude of 2.8 V/cm.

where we have defined the zero of energy as the energy of the $(n+2)s$ state in zero electric field. W_o is the energy of the $n,3$ state in zero field, k is the dipole moment of the $n,3$ state, and α^S is the scalar polarizability of the $(n+2)s$ state; these parameters can be determined by diagonalizing the Stark Hamiltonian with a finite basis [15]. For the $22,3$ and $24s$ states $W_o/2\pi=110.4$ GHz, $k/2\pi=815.5$ MHz/(V/cm), and $\alpha^S/2\pi=0.5127$ MHz/(V/cm)². Near the crossing the states have a relative slope $k_{\text{rel}}/2\pi$ of 750 MHz/(V/cm), where $k_{\text{rel}}=k-\alpha^S E_{\text{DC}}$. In the absence of coupling, these states would cross at 141.7 V/cm.

As evidenced by the small avoided crossing in Fig. 1(a), the states are coupled by interaction with the nonhydrogenic atomic core. Off-diagonal matrix elements mix the two states and cause the crossing to be avoided with size Ω_o . The upper and lower energy levels in the diagram are referred to as the adiabatic states; far from the avoided crossing they are identifiable as the diabatic states, but near the crossing they are strongly mixed. Because the d and p states are isolated from the Stark manifold at the electric field where the $(n+2)s$ and $n,3$ states intersect, the $(n+2)s$ state is only weakly coupled to the high- ℓ states in the manifold, leading to a particularly small avoided crossing. The size of these crossings scale as n^{-6} , and for the $24s$ to $22,3$ states we numerically calculated $\Omega_o/2\pi=139$ MHz.

The coupling between the $(n+2)s$ and $n,3$ states due to an rf field is given by the multiphoton Rabi rate, which can be derived from Floquet theory [16]

$$\Omega_n = \Omega_o J_n \left(\frac{(k - \alpha^S E_{\text{DC}}) E_{\text{rf}}}{\omega_{\text{rf}}} \right), \quad (1.2)$$

where $J_n(x)$ is a Bessel function. Thus, the multiphoton Rabi rate is predictable from static atomic properties, a precisely

measurable static electric field E_{DC} , the amplitude E_{rf} , and the frequency ω_{rf} of the rf pulse. In weak rf fields, where $k_{\text{rel}} E_{\text{rf}} \ll \omega_{\text{rf}}$, these couplings are identical to the perturbative limit of $\Omega_n \propto E_{\text{rf}}^n$. Most of our data was taken in the regime where the energy levels are strongly perturbed by the rf field, $k_{\text{rel}} E_{\text{rf}} \gg \omega_{\text{rf}}$. Previous CHIRAP experiments using lasers [4,6,7,10,11] were performed with intensities that gave (ac Stark) energy-level shifts significantly smaller than the photon energy [17–19].

These two levels of potassium are an excellent system for exploring multiphoton transitions. A combination of small multiphoton Rabi rates (less than 100 MHz) and the relative slopes near 1 GHz/(V/cm) of the two states makes them ideal for experiments using the Floquet picture in the frequency range near 1 GHz with amplitudes of less than 10 V/cm. Fields in this frequency and amplitude range can be readily produced and controlled in the laboratory. In addition, measurement of the population of both of the states can be done with high efficiency through selective electric-field ionization [20].

Below we describe the experimental apparatus and the procedures for measuring the pulse parameters and data for the population transfer. Next, we discuss the results of the experiment and compare our results to a Floquet model. The Floquet model [21] of multiphoton transitions has been used extensively in the analysis of multiphoton laser [17–19,22–25] and microwave [16,26–28] experiments. In laser experiments the theory is understandably difficult to check, because of the necessity of focusing the laser and the strong dependence of the predictions on the field strength [17,19,25].

II. EXPERIMENT

The experiments were designed to measure the transition probability for transitions between the $(n+2)s$ and $n,3$ states in potassium driven by chirped rf fields as a function of the chirp, the rf intensity, and the photon order. Here, we briefly give an overview of the experiment, followed in subsequent paragraphs by a detailed description of the various parts of the apparatus. A thermal beam of potassium atoms passes between the parallel plates of a $50\ \Omega$ transmission line, shown schematically in Fig. 2. Lasers excite the atoms to the lower level of the two-level system. The rf pulse is generated by a voltage-tuned oscillator (VTO), the output of which is gated with rf mixers, attenuated to set the rf amplitude, then amplified and coupled into the transmission line. The atoms then undergo multiphoton transitions to the upper level. Finally, the populations in the two states are detected by a selective field ionization pulse applied to the lower plate of the transmission line.

The transmission line is of a similar design to one described earlier [29,30]. The line consists of two parallel brass plates with a width to separation ratio of 7.5 , so that they have a $50\text{-}\Omega$ impedance. In this 20-cm -long transmission line, the plate separation is 0.762 cm, and the width of the plates is 5.72 cm. The signal to the top plate is coupled from a coaxial cable by standard SMA connectors and passes to a monitor via a second SMA connector and coaxial cable. The

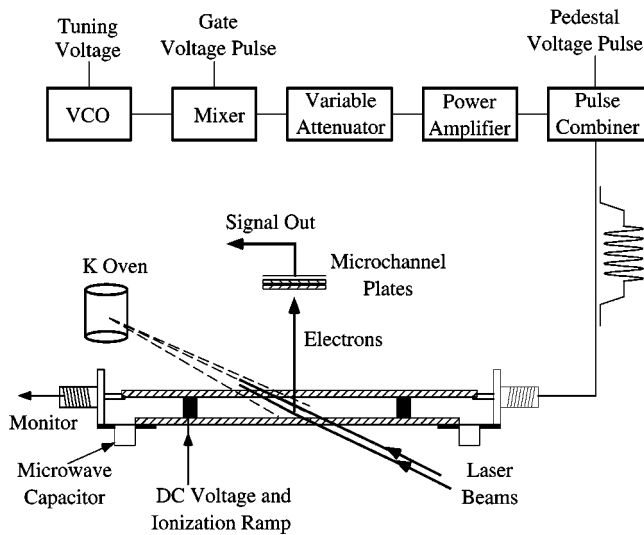


FIG. 2. Overview of the experimental apparatus showing the chirped-pulse generation scheme, parallel-plate transmission line, atomic source, and microchannel plate detectors. The atomic and laser beams are antiparallel with the laser polarization in the vertical direction. The transmission line is constructed of brass with SMA connectors and 100-pF capacitors used to couple the pedestal and microwave pulses onto the line while isolating the bottom plate from ground to allow static and state-selective field ionization pulses to be applied. A 0.5-mm hole drilled in the top plate of the transmission line allows electrons from the ionized atoms to reach the detector.

lower plate is connected to the SMA grounds via 100-pF microwave capacitors. The capacitors allow the application of static voltages and slowly varying high-voltage ramps to the lower plate while only minimally affecting the transmission of the rf. Care was taken to minimize the reflection of the rf at the interface between the coaxial lines and the parallel-plate transmission line. In order to reduce static field inhomogeneities, the plates of the transmission line were carefully flattened, polished, coated with carbon, and drilled with a single 0.5-mm hole in the top plate through which electrons could pass.

The atomic beam is produced in a resistively heated oven and passes through the transmission line perpendicular to the propagation of the rf pulse. The atoms are excited in a step-wise manner, from the $4s_{1/2}$ to the $4p_{3/2}$ and then to the selected $(n+2)s$ Rydberg states by two pulsed homebuilt nanosecond dye lasers pumped, respectively, by the second and third harmonics of a 20-Hz Nd:YAG (yttrium aluminum garnet) laser. The excitation takes place in a static electric field about 134 V/cm, well below the avoided crossing shown in Fig. 1(a). This electric field is produced by applying a well-regulated negative voltage to the bottom plate. The laser beams are nearly colinear and propagate antiparallel to the atomic beam.

About 100 ns after the Rydberg state is populated, a “pedestal” voltage is applied that brings the states to the field required for the experiment. The pedestal voltage slowly increases the electric field, in a time of about $2 \mu\text{s}$, by adding a voltage of up to +8 V to the top plate of the transmission line; the amplitude of this voltage is computer controlled.

The pedestal voltage remains constant for $2 \mu\text{s}$, during which time the rf pulse is applied, and then falls back to zero in an additional $2 \mu\text{s}$. The pedestal voltage is coupled into the rf circuit with a modified bias tee (Pasternack PE-1601). Over $1 \mu\text{s}$ the top of the pedestal voltage is constant to better than 1% ($<0.08 \text{ V}$).

Using the pedestal voltage allows the laser excitation to take place well away from the avoided crossing where the states are mixed, and thus only excite the lower level. Laser excitation near the avoided crossing populates a superposition of both the upper and lower states. However, because the dynamics within the pedestal voltage are entirely adiabatic, population remains exclusively in the lower level, independent of how close to the avoided crossing the states are brought.

Approximately 500 ns after the pedestal voltage returns to zero, a large, negative, ramped voltage with a rise time of $1 \mu\text{s}$ applied to the bottom plate ionizes the atoms. Electrons produced by field ionization are then detected by a microchannel plate detector, with the electrons from the $n,3$ state arriving 50 ns before those from the $(n+2)s$ state. The technique of using the pedestal voltage has the additional advantage of keeping the time of field ionization constant for each state, even for experiments, such as those shown in Fig. 1(b), where the energy separation is changed. The signal from the microchannel plates is then amplified and averaged in a gated integrator. The output of the gated integrator is read by a digital-to-analog converter and the data is transferred to a computer.

The rf source was a Avantek VTO-9068 voltage-tuned oscillator designed specifically for fast frequency hopping between 500 and 1000 MHz. The output power of this device is 10 dBm, and the frequency is tuned by biasing a voltage variable capacitor (varactor). The VTO’s tuning rate is limited mainly by the output impedance of the circuit driving the capacitive load of the varactor. In cw mode, the oscillator is tuned with a regulated dc power supply. In chirped-pulse operation, the oscillator is tuned by altering the capacitance of the varactor with a ramped voltage. The ramp to the varactor is created by an HP8015A pulse generator, which has a variable rise time output that is controlled with a computer. The output of the HP8015A is buffered by a fast, low output-impedance amplifier (CLC430) that in turn drives the varactor.

The output of the oscillator is sent to a pair of broadband mixers (Minicircuits ZFM-4H) whose intermediate frequency ports are driven by the output of an SRS DG535 pulse generator. This provides a pulse of rf with a controllable width that has an on-off contrast ratio of 42 dB. The output of the mixers is a trapezoidal pulse of rf with a rise time of 3 ns. This output is sent to a set of step attenuators and finally to a broadband power amplifier (MiniCircuits ZHL-2-12) with a maximum output power of 27 dBm. The output of the amplifier is then sent to the rf input of the bias tee and from there to the transmission line. The rf pulses are timed to arrive at the transmission line during the peak of the pedestal voltage.

The simplest experiment using the apparatus measures population transfer for a pulse with constant frequency as a

function of the static electric field, which corresponds to measurement of absorption versus the energy separation between the two quantum states. By varying the dc field from 136 to 142 V/cm, one to five photon resonance with a 750-MHz pulse can be produced for the energy levels seen in Fig. 1(a). Figure 1(b) shows the population transfer from the lower to upper levels as a function of static electric field for a $1 \mu\text{s}$ pulse of 750-MHz radiation. This figure clearly shows that absorption comes when the energy separation is an integer times the photon energy [14,20]. Because the upper state does not have definite parity both even- and odd-order processes are allowed. For low-intensity pulses only the single-photon transition has appreciable probability, while with the 2.8 V/cm rf field strength used for the experiment Fig. 1(b), up to five photons of absorption can be easily seen.

Data such as those in Fig 1(b) also allow us to estimate the static field homogeneity within the transmission line. The width of the five-photon resonance in Fig. 1(b) is 0.08 V/cm, demonstrating a static field homogeneity of better than 0.05%. The inhomogeneity of the field is probably mostly due to variations in the pedestal voltage, but there is certainly a contribution from imperfections in the transmission line plates. Such a field homogeneity gives an uncertainty in the resonance frequency of $k_{\text{rel}}\Delta E_{\text{DC}} \approx 60$ MHz.

We calibrate the rf field amplitude in two ways, and these methods agree to within 5%. First, and most simply, we measure the voltage between the plates of the transmission line using a high-impedance fast oscilloscope probe (Avtech AVP-BP-1) and a digital sampling oscilloscope with a 1.5-GHz bandwidth. Using this voltage and the known spacing between the plates of the transmission line we determined a calibration between the attenuation and the rf amplitude in the interaction region. Because of the inevitable reflections and cable losses, this method is significantly more accurate than measurements made by sampling the voltage entering or leaving the transmission line.

The second method we used, initially to determine the accuracy of the oscilloscope probe, is to use the known one-photon Rabi rates [16] and to calibrate by measuring the population transfer as a function of the width of the rf pulse. This method has turned out to be remarkably accurate and was the method used for field calibration in all of the chirped-pulse experiments to be presented in Sec. III.

For a given resonance frequency ω_o and rf frequency ω_{rf} , the population will oscillate between the two states as a function of time given by the familiar Rabi equation

$$P(t) = \frac{\Omega_n^2}{\Omega_n^2 + \Delta_n^2} \sin^2 \left(\sqrt{\Omega_n^2 + \Delta_n^2} \frac{t}{2} \right), \quad (2.1)$$

where $\Delta_n = n\omega_{\text{rf}} - \omega_o$ is the detuning from multiphoton resonance and the Rabi rate Ω_n is given by Eq. (1.2). In the calibration experiment, we invert this equation and determine the strength of the rf field from the measured Rabi rate, assuming zero detuning. First, the rf oscillator is set to 750 MHz, and the pedestal voltage brings the electric field to the

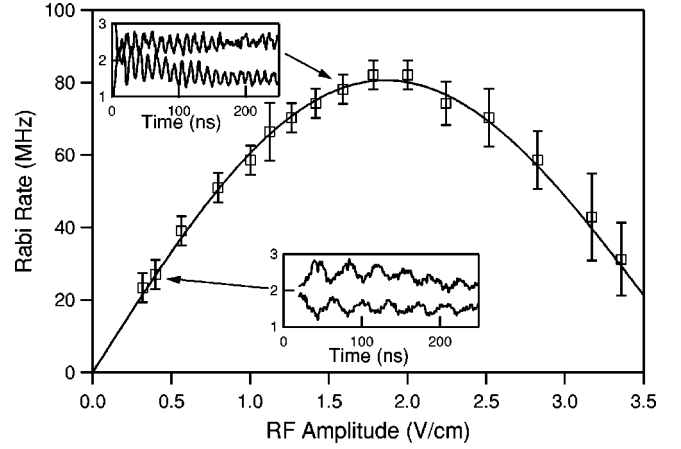


FIG. 3. Rabi rate measured for the one-photon transition between the $24s$ state and the $19,3$ state. The solid line is a fit to Eq. (1.2). The inset figures show the measured electron signal (in arbitrary units) for each state as a function of rf pulse width for the two points indicated on the graph.

position of the one-photon resonance, determined by a scan similar to that in Fig. 1(b), but taken with very low rf amplitude (≈ 5 mV/cm) so as to determine the location of the resonance accurately.

An rf pulse with a variable width is applied and the population is measured as a function of pulse width and pulse intensity. Data from this experiment is shown in Fig. 3. The inset figures show the electron signals from the $24s$ and $22,3$ field ionization for two different rf amplitudes as a function of pulse width.

Data such as these were Fourier transformed and the oscillation frequencies were determined. A series of sets of data were taken in this way and the extracted Rabi rates were plotted. The error bars in Fig. 3 are the full width at half maximum of the peaks in the Fourier transforms. Equation (1.2) was fit to the data using a scale factor for the rf amplitude as the only parameter. The data agrees with the theory and the extracted field calibration is within 5% to the rf amplitudes determined with the oscilloscope probe.

In chirped-pulse operation, the frequency can be swept from 675 to 825 MHz in as little as 15 ns. We have experimentally determined that the frequency follows the applied voltage faithfully, even when using the fastest rise time pulses that we can apply. We have measured the properties of the chirped pulses with the fast oscilloscope probe and digital oscilloscope; an example of a fast sweep is displayed in Fig. 4(a) for an 80-ns pulse swept from 675 to 825 MHz. To extract the time dependence of the rf frequency we have used the method of complex demodulation [31]. Complex demodulation extracts the amplitude and phase as a function of time relative to a carrier wave. Figure 4(b) shows the phase of the measured pulse relative to a 750-MHz carrier wave as a light line.

Determining the frequency as a function of time from the phase data can be done with a numerical derivative or by fitting the phase function to a known shape. For slow sweeps, (not shown) with a sweep time of greater than 50 ns, the frequency is essentially a linear function of time, except

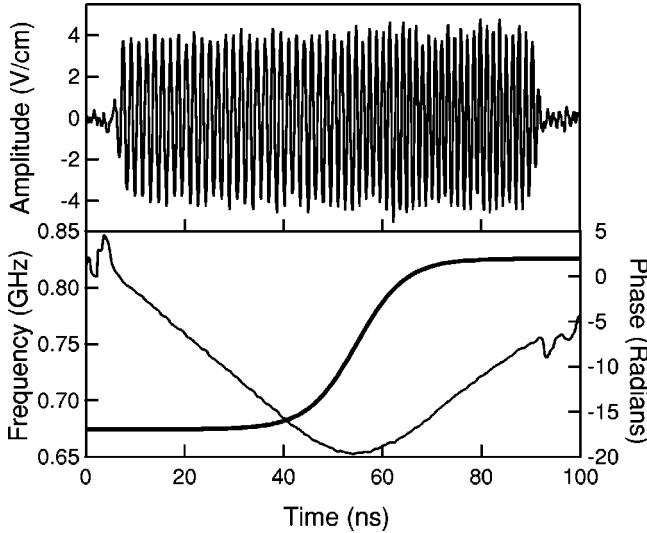


FIG. 4. Data from a sample chirped rf pulse showing (a) the actual rf field versus time in the transmission line and (b) a measurement of the phase relative to a 750-MHz carrier (light line) and the instantaneous frequency (dark line) of the pulse assuming a hyperbolic tangent shape.

very close to the beginning and end of the sweep. For faster sweeps, such as the one shown in Fig. 4, the frequency is not a linear function of time and its shape can be modeled by a hyperbolic tangent,

$$\omega(t) = \omega_o + \beta \tanh\left(\frac{t-t_o}{\tau}\right), \quad (2.2)$$

where β determines the extent of the frequency sweep and τ is a measure of the rise time. After fitting the phase extracted from the complex demodulation to the equation

$$\phi_{\text{rel}}(t) = +\beta\tau \ln\left[\cosh\left(\frac{t-t_o}{\tau}\right)\right] + C, \quad (2.3)$$

we determine $\omega(t) = \omega_o + d\phi_{\text{rel}}/dt$, as is shown by the bold line in Fig. 4(b).

In the analysis of Sec. III, we treat the frequency sweep as if it were completely linear, but for the fastest sweeps, typified by the data in Fig. 4, this is clearly not the case. However, if the rf is near resonant in the middle of the sweep, $t \approx t_o$, the frequency is approximately linear in time, $\omega = \omega_o + \beta(t-t_o)/\tau$. In our fastest sweeps, this linear region extends over approximately 100 MHz of the 150-MHz sweep. As long as the multiphoton Rabi rate is smaller than the interval over which the frequency changes linearly, which is the case for all of the data we present, then we can use β/τ as an effective linear chirp rate.

III. RESULTS AND DISCUSSION

We have measured the transition probability for multiphoton transitions as a function of the chirp, keeping the rf amplitude constant. Typical data for the $24s$ to $22,3$ transition are shown as the open circles in Fig. 5. In these graphs and in the analysis that follows, we define the chirp of our pulses as

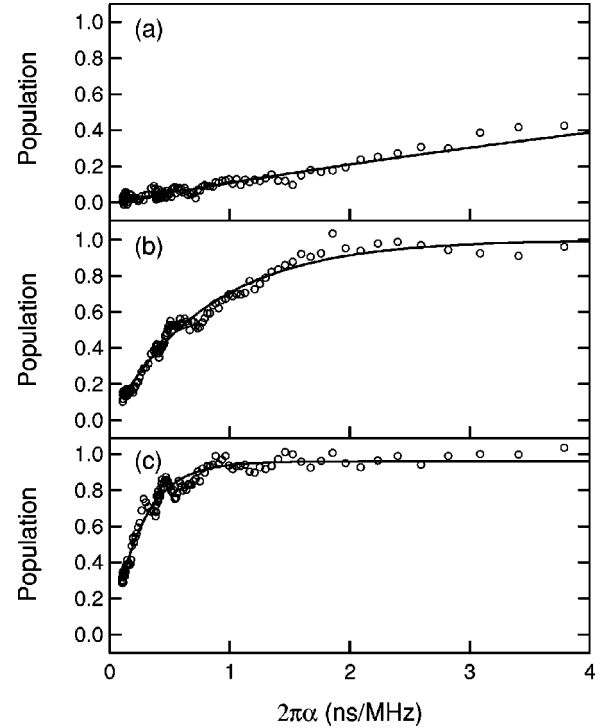


FIG. 5. Plot of the experimental data (circles) of the upper-state population as a function of the chirp $2\pi\alpha$ for four-photon transitions between the $24s$ and $22,3$ states. The three graphs show the effect of varying the field strength of the chirped pulses. From top to bottom the data are for (a) 2.3 V/cm ($\Omega_4/2\pi=7$ MHz), (b) 3.3 V/cm ($\Omega_4/2\pi=23$ MHz), and (c) 5.8 V/cm ($\Omega_4/2\pi=53$ MHz). The solid lines are fits of the Landau-Zener equation, Eq. (3.4), to the data, from which the multiphoton Rabi rates may be extracted.

$\alpha = 1/\dot{\omega}$. This designation, following the spirit of Noordam and co-workers [4,7], makes both the analysis to follow and the insensitivity of full population transfer to exact parameters of the pulse more clear.

Data was recorded as the rf was chirped over a frequency interval $\Delta f = 150$ MHz from 675 to 825 MHz in a time interval Δt , which was varied between 15 ns and 600 ns, corresponding to chirps $2\pi\alpha = \Delta t/\Delta f$ of 0.1 ns/MHz to 4 ns/MHz. By varying the rf field we vary the coupling between the two levels allowing observation of the effect of the multiphoton Rabi rate on the population transfer.

Data such as that shown in Fig. 5 has been taken with the frequency swept in both directions, either increasing (red to blue) or decreasing (blue to red) the frequency during the rf pulse. The data are identical for these experiments, as is expected for two-level systems. All data presented in this paper were taken using red-to-blue sweeps. Experiments were also performed with $\Delta f = 100$ and 200 MHz with indistinguishable results.

The data in Fig. 5 show qualitatively how the population transfer depends both on the chirp and the amplitude of the rf pulse. Figure 5(a) shows data for a weak pulse, with an rf amplitude of 2.3 V/cm, corresponding to a Rabi rate $\Omega_n/2\pi = 7$ MHz. In this regime the population transfer is linearly proportional to the chirp or, equivalently, to the time the chirped pulse spends near resonance. For the data in

Figs. 5(b) and 5(c), corresponding to Rabi rates of $\Omega_n/2\pi = 23$ MHz and $\Omega_n/2\pi = 53$ MHz, respectively, the data increases linearly at small chirp and then saturates with 100% population transfer. The data also shows small oscillations superimposed on the overall structure.

In order to understand the data, we define an effective pulse area as the product of the on-resonance Rabi rate multiplied by the time spent within $\pm \Omega_n/2$ of the resonant frequency,

$$A_{\text{eff}} = \Omega_n \left(\frac{\Omega_n}{n\Delta\omega} \Delta t \right) = \frac{\Omega_n^2}{n\dot{\omega}} = \Omega_n^2 \frac{\alpha}{n}, \quad (3.1)$$

where $\Delta\omega = 2\pi\Delta f$, $\dot{\omega}$ is the constant rate of change of the angular frequency, and $\alpha = 1/\dot{\omega}$ is the linear chirp.

The response will be described well by perturbation theory as long as the effective pulse area is much less than π . For a weak broadband pulse, we expect that the transfer probability is given by [32]

$$|C_2|^2 = P_{\text{trans}} = \frac{\pi}{2} \Omega_n^2 \frac{\Delta t}{\Delta\omega} = \frac{\pi}{2} A_{\text{eff}}. \quad (3.2)$$

In the perturbative regime the population transfer is expected to be linearly proportional to the chirp.

In the case of the data in Fig. 5(a) the n -photon detuning $n\Delta$ is less than the Rabi rate for 5 ns at the slowest chirp, giving a pulse area $A_{\text{eff}} \approx 0.3$. Thus, the perturbative result of Eq. (3.2) agrees with the data presented in Fig. 5(a).

Figures 5(b) and 5(c) show that when the rf pulses are more intense, with a commensurate rise in the Rabi rate, that the population transfer is no longer a linear function of the chirp, and that a simple perturbative analysis no longer holds. For pulses such as these, where the Rabi rates are so large that the effective pulse areas A_{eff} are greater than π for pulses with slow chirp rise times. In the graphs of Figs. 5(b) and 5(c), $A_{\text{eff}} = \pi$ for $2\pi\alpha = 3.8$ ns/MHz and $2\pi\alpha = 0.7$ ns/MHz, respectively.

In order to analyze the data for large intensities and relatively slow chirps we have used the dynamic Floquet model [16]. The Floquet model determines the energy levels of dressed states, and converts the problem of the two levels interacting with a rapidly oscillating field to one that is formally identical to that of the dynamics of two real energy levels with an avoided crossing of size Ω_n and a separation governed by the rf frequency. The location of the avoided crossing is the rf frequency for n -photon resonance, and the size of the avoided crossing is adjustable by the experimentally controllable rf amplitude. Written in matrix form, Schrödinger's equation for the evolution of the Floquet states of the two-level system is given by

$$i \begin{pmatrix} \dot{c}_1 \\ \dot{c}_2 \end{pmatrix} = \begin{pmatrix} W_1 & \frac{\Omega_n}{2} \\ \frac{\Omega_n}{2} & W_2 - n\omega_{\text{rf}} \end{pmatrix} \begin{pmatrix} c_1 \\ c_2 \end{pmatrix}, \quad (3.3)$$

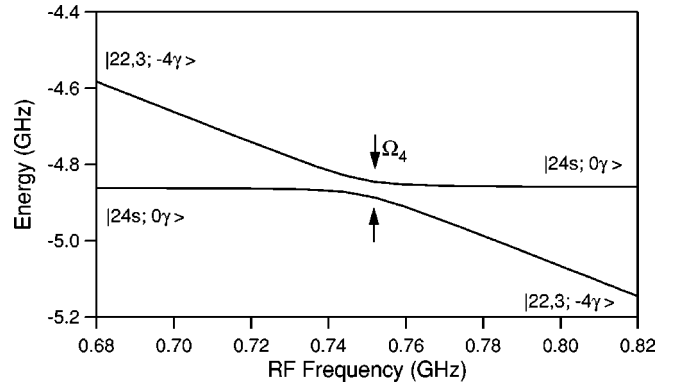


FIG. 6. Floquet energies of the 24s and 22,3 states as a function of rf frequency near the four-photon resonance at 750 MHz. The figure was calculated for $E_{\text{rf}} = 4$ V/cm, corresponding to a multiphoton Rabi rate of 40 MHz. For frequencies far from resonance the energy levels are identifiable with the dressed diabatic states, but near the avoided crossing the states are strongly mixed.

where the energies, W_1 and W_2 are defined in Eq. (1.1) and $W_2 - n\omega_{\text{rf}}$ is the energy of the $n,3$ state, shifted downward by the energy of n photons. The off-diagonal matrix element is given by Eq. (1.2). The eigenvalues of the Hamiltonian of Eq. (3.3) are plotted as a function of frequency in Fig. 6 for the example case of the four-photon crossing for $n = 22$.

Use of the dynamic Floquet model requires that the rf frequency be much greater than the Rabi rate, $\omega_{\text{rf}} \gg \Omega_n$. It further requires that the frequency excursions be small compared to the rf frequency $n\Delta\omega \ll \omega_{\text{rf}}$, so that only a single multiphoton resonance contributes to the population transfer. Also, the dynamic Floquet theory breaks down if some of the characteristics of the pulse (amplitude, frequency, phase) change on a time scale fast compared to the rf frequency. An interesting question is whether the chirped pulses we create, with frequency sweep times of only a few cycles, enter the regime where the dynamic Floquet theory fails to describe the result.

In a very weak rf field these two Floquet states nearly cross at the resonance frequency, and sweeping the rf frequency through the resonance transfers very little population. On the other hand if the Rabi rate is large, the avoided crossing will be significant. For slowly changing rf frequencies, an atom initially in the lower-level atom will adiabatically follow the lower state as the frequency increases, with all of the population transferring from the $(n+2)s$ state to the $n,3$ state.

For all chirps and avoided crossing sizes the fraction of the population transferred to the upper level can be determined by calculating the evolution of Eq. (3.3). However, for linear chirps, the population transfer calculated from Eq. (3.3) is the well-known result of Landau and Zener [33,34]. In this case, the probability of making a transition P_{trans} between the upper and lower states is given by

$$P_{\text{trans}} = 1 - \exp\left(-\frac{\pi}{2} \frac{\Omega_n^2}{n\dot{\omega}_{\text{rf}}}\right) = 1 - e^{-(\pi/2)A_{\text{eff}}}. \quad (3.4)$$

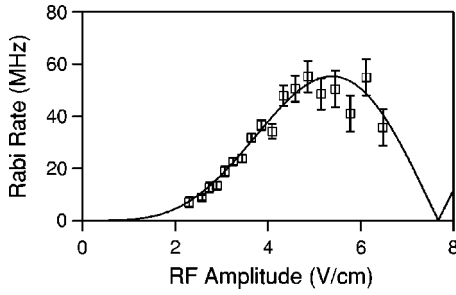


FIG. 7. Multiphoton Rabi frequency $\Omega_n/2\pi$ as a function of rf amplitude for the four-photon transition between $24s$ and $22,3$. The rates were extracted from scans like those in Fig. 5 and are compared to the theoretical values of Eq. (1.2).

The transition probability given here depends exponentially on the effective area of the pulse, defined in Eq. (3.1). For small values of A_{eff} this gives the same answer as Eq. (3.2).

In order to compare the data to the Landau-Zener predictions of the adiabatic Floquet model we fit the data to the form of Eq. (3.4) to determine the multiphoton Rabi rates. The equations for these Rabi rates are well established by direct measurement [16,28,35] as was done in Fig. 3. In addition to the Rabi rates the fits also included two other parameters, a baseline offset and a scale factor to allow conversion between the electron signal and transition probability. Errors in the Rabi rate were assigned by performing several experiments at each rf power level.

Many such data sets were acquired for different values of the rf field strength, for different photon order, and for different principal quantum number. Data for the four photon $24s$ to $22,3$ transition is summarized in Fig. 7 along with the theoretically predicted value of the Rabi rate given by Eq. (1.2). Agreement is quite good, showing that the Landau-Zener formula does a good job of predicting population transfer for these multiphoton transitions.

We have also looked at different order processes and extracted Rabi rates for the 2, 3, 4, and 5 photon transitions between the $21s$ and $19,3$ states are shown in Fig. 8. Also shown in Fig. 8 is the theoretically predicted values of the Rabi rates for the different photon orders as predicted by Eq.

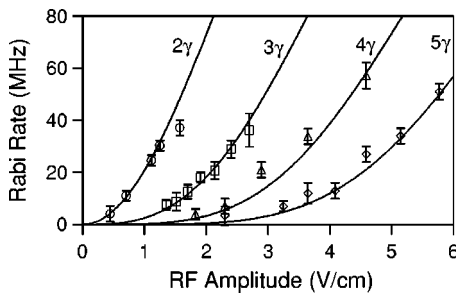


FIG. 8. Multiphoton Rabi frequency $\Omega_n/2\pi$ determined from the Landau-Zener model as a function of rf amplitude for transitions of a variety of different photon orders. The data for these Rabi rates are for transitions between the $21s$ and $19,3$ states. The solid lines are calculated from Eq. (1.2).

(1.2). Again, agreement between the Landau-Zener predictions and the measured transition probabilities is quite good.

For the $21s$ to $19,3$ transition we are unable to see the maximum in the Bessel function dependence of Eq. (1.2). The limits on the fastest frequency sweeps that we can achieve in the apparatus limit us to a maximum Rabi rate that can be measured. In order to fit the data to a meaningful Landau-Zener curve, the population transfer must change significantly over the range of chirps available. We can estimate the maximum Rabi rate that we can measure by requiring that at least the population in the final state vary from 0 to $1/2$ or from $1/2$ to 1. This sets the maximum measurable value of Ω_n as

$$(\Omega_n)_{\text{lim}} = \sqrt{\frac{4n \ln(2)}{2\pi\alpha}}. \quad (3.5)$$

In practice this equation has given a good estimate of the range of Rabi frequencies that we can measure: from $4\sqrt{n}$ MHz to $25\sqrt{n}$ MHz.

Despite the agreement between theory and experiment, there are several features of the experiment that could affect the use of the Landau-Zener model of the data. We address these below. First, the fastest chirps produces shifts in the energy levels that do not sweep linearly with time, as was assumed in the derivation of Eq. (3.4). Rubbmark *et al.* [36] did extensive calculations of corrections to the Landau-Zener formula, showing that as long as the total multiphoton frequency excursion $n\Delta\omega$ is much greater than the avoided crossing size, there is only a small difference between the Landau-Zener prediction and the actual population transfer. In a related analytical calculation McIlrath *et al.* [37] considered both the linear and quadratic terms in the rate of change in the states' energies. They showed that the linear term in the Landau-Zener model dominates the behavior even when the curvature is significant.

As discussed by Vrijen *et al.* [23] in order for the Landau-Zener approximation to be used, there is a second criterion that must be met, namely, that the coupling between the states is negligible far from resonance. Vrijen *et al.* showed that, for high-order multiphoton processes that were shifted through resonance by the ac Stark shift, this second criterion does not hold for high-order processes. If the Rabi rate grows faster than the detuning, the off-resonance coupling can be large enough that there is significant transition probability far from resonance, leading to disagreement with the predictions of Eq. (3.4). In our experiment the use of Eq. (3.4) is predicated on the fact that the detuning $n\Delta$ at the beginning and the end of the pulse is significantly greater than the maximum Rabi rate.

Finally, in addition to the small deviations from linear chirp near the resonance, Eq. (1.2) shows that the Rabi rate changes as the rf frequency is swept through resonance. In order to use the Landau-Zener model, we have treated the Rabi rate as a constant. Ω_n varies with frequency as $\Omega_n/\omega_{\text{rf}}$, and the variation is quite small across the values of ω_{rf} for which the states are strongly interacting. Further, the ap-

proximation agrees when compared with direct numerical integration of Schrödinger's equation for the system without using the Floquet model.

As mentioned above, the data in Fig. 5 show small oscillations in the population transfer in addition to the overall Landau-Zener behavior. We attribute these to a combination of two causes: resonances that are not centered exactly in the middle of the frequency sweep combined with the fast turn on of the rf pulse. If the atoms are closer to resonance at either the beginning or the end of the pulse there can be a significant amplitude for Rabi flopping while the pulse is off resonance. Were the rise time of the rf field strength longer than its current 3 ns, these Rabi oscillations would be washed out and not be visible. This conjecture is supported by numerical studies of Eq. (3.3).

IV. CONCLUSIONS

We have presented a study of the interaction of intense frequency-swept pulses interacting with a two-level atom. The data in Fig. 5 can be compared to experiments done by Rubbmark *et al.* [36]. In these experiments they measured

the population transfer between two states in a rapidly slewing electric field. We are able to tune the size of the avoided crossing with the strength of the rf field and thus can see both completely diabatic and completely adiabatic behavior. This allows the observation of the Landau-Zener curve over its full range, not just in the limit of adiabatic passage.

By adjusting the amplitude and frequency sweep rate we have been able to compare the results of the experiment to the predictions of the dynamical Floquet model, and the Landau-Zener analysis of the frequency swept pulses interacting with the atoms. We have shown that this model works very well in describing the effect of the pulse on the atoms despite the large chirps and the deviations from linearity of the chirp. Understanding such systems is an important step in developing procedures that control the dynamics of more complex systems.

ACKNOWLEDGMENTS

We would like to thank Robert Jones, Tom Gallagher, and Bart Noordam for useful discussions.

-
- [1] B. W. Shore, K. Bergmann, A. Kuhn, S. Schieman, J. Oreg, and J. H. Eberly, *Phys. Rev. A* **45**, 5297 (1992).
 - [2] V. S. Malinovsky and D. J. Tannor, *Phys. Rev. A* **56**, 4929 (1997).
 - [3] N. V. Vitanov, B. W. Shore, and K. Bergmann, *Eur. Phys. J. D* **4**, 15 (1998).
 - [4] B. Broers, H. B. van Linden van den Heuvell, and L. D. Noordam, *Phys. Rev. Lett.* **69**, 2062 (1992).
 - [5] J. S. Melinger, S. R. Gandhi, A. Hariharan, J. X. Tull, and W. S. Warren, *Phys. Rev. Lett.* **68**, 2000 (1992).
 - [6] P. Pillet, C. Valentin, R.-L. Yuan, and J. Yu, *Phys. Rev. A* **48**, 845 (1993).
 - [7] P. Balling, D. J. Maas, and L. D. Noordam, *Phys. Rev. A* **50**, 4276 (1994).
 - [8] Y. B. Band and O. Magnes, *Phys. Rev. A* **50**, 584 (1994).
 - [9] J. S. Melinger, D. McMorrow, C. Hillegas, and W. S. Warren, *Phys. Rev. A* **51**, 3366 (1995).
 - [10] C. Bardeen, V. V. Yakovlev, K. R. Wilson, S. D. Carpenter, P. M. Weber, and W. S. Warren, *Chem. Phys. Lett.* **280**, 151 (1997).
 - [11] D. J. Maas, D. I. Duncan, A. F. G. van der Meer, W. J. van der Zande, and L. D. Noordam, *Chem. Phys. Lett.* **270**, 45 (1997).
 - [12] S. Guérin, *Phys. Rev. A* **56**, 1458 (1997).
 - [13] T. F. Gallagher, *Rydberg Atoms* (Cambridge University Press, Cambridge, 1994).
 - [14] L. A. Bloomfield, R. C. Stoneman, and T. F. Gallagher, *Phys. Rev. Lett.* **57**, 2512 (1986).
 - [15] M. L. Zimmerman, M. G. Littman, M. M. Kash, and D. Kleppner, *Phys. Rev. A* **20**, 2251 (1979).
 - [16] M. Gatzke, M. C. Baruch, R. B. Watkins, and T. F. Gallagher, *Phys. Rev. A* **48**, 4742 (1993).
 - [17] R. B. Vrijen, J. H. Hoogenraad, H. G. Muller, and L. D. Noordam, *Phys. Rev. Lett.* **70**, 3016 (1993).
 - [18] D. I. Duncan, J. G. Story, and T. F. Gallagher, *Phys. Rev. A* **52**, 2209 (1995).
 - [19] R. R. Jones, *Phys. Rev. Lett.* **74**, 1091 (1995).
 - [20] R. C. Stoneman, D. S. Thomson, and T. F. Gallagher, *Phys. Rev. A* **37**, 1527 (1988).
 - [21] J. H. Shirley, *Phys. Rev.* **138**, B979 (1965).
 - [22] J. G. Story, D. I. Duncan, and T. F. Gallagher, *Phys. Rev. Lett.* **70**, 3012 (1993).
 - [23] R. B. Vrijen, J. H. Hoogenraad, and L. D. Noordam, *Mod. Phys. Lett. B* **8**, 205 (1994).
 - [24] J. G. Story, D. I. Duncan, and T. F. Gallagher, *Phys. Rev. A* **50**, 1607 (1995).
 - [25] R. R. Jones, *Phys. Rev. Lett.* **75**, 1491 (1995).
 - [26] M. C. Baruch and T. F. Gallagher, *Phys. Rev. Lett.* **68**, 3515 (1992).
 - [27] M. Gatzke, R. B. Watkins, and T. F. Gallagher, *Phys. Rev. A* **51**, 4835 (1995).
 - [28] M. W. Noel, W. M. Griffith, and T. F. Gallagher, *Phys. Rev. A* **58**, 2265 (1998).
 - [29] C. W. S. Conover and J. H. Rentz, *Phys. Rev. A* **55**, 3787 (1997).
 - [30] C. W. S. Conover and M. C. Doogue, *Phys. Rev. A* **63**, 032504 (2001).
 - [31] P. Bloomfield, *Fourier Analysis of Time Series: An Introduction* (Wiley, New York, 1976).
 - [32] R. Loudon, *The Quantum Theory of Light* (Oxford University Press, Oxford, London, 1983).
 - [33] C. Zener, *Proc. R. Soc. London, Ser. A* **137**, 696 (1932).
 - [34] L. Landau, *Phys. Z. Sowjetunion* **2**, 46 (1932).
 - [35] L. Ko, M. W. Noel, J. Lambert, and T. F. Gallagher, *J. Phys. B* **32**, 3469 (1999).
 - [36] J. R. Rubbmark, M. M. Kash, M. G. Littman, and D. Kleppner, *Phys. Rev. A* **23**, 3107 (1981).
 - [37] T. J. McIlrath, R. R. Freeman, W. E. Cooke, and L. D. van Woerkom, *Phys. Rev. A* **40**, 2770 (1989).